ELSEVIER

NeuroImage

www.elsevier.com/locate/ynimg
NeuroImage 32 (2006) 626 – 636

Hierarchical microimaging for multiscale analysis of large vascular networks

Stefan Heinzer,[a] Thomas Krucker,[b] Marco Stampanoni,[c] Rafael Abela,[c] Eric P. Meyer,[d] Alexandra Schuler,[d] Philipp Schneider,[a] and Ralph Müller[a,*]

[a] *Institute for Biomedical Engineering, University and ETH Zürich, Zürich, Switzerland*
[b] *Central Technologies, Novartis Institutes for BioMedical Research (NIBRI), Cambridge, MA 02139, USA*
[c] *Swiss Light Source (SLS), Paul Scherrer Institut (PSI), 5232 Villigen, Switzerland*
[d] *Department of Neurobiology, Institute of Zoology, University of Zürich, Zürich, Switzerland*

Received 1 December 2005; revised 15 February 2006; accepted 23 March 2006
Available online 11 May 2006

There is a wide range of diseases and normal physiological processes that are associated with alterations of the vascular system in organs. Ex vivo imaging of large vascular networks became feasible with recent developments in microcomputed tomography (μCT). Current methods permit to visualize only limited numbers of physically excised regions of interests (ROIs) from larger samples. We developed a method based on modified vascular corrosion casting (VCC), scanning electron microscopy (SEM), and desktop and synchrotron radiation μCT (SRμCT) technologies to image vasculature at increasing levels of resolution, also referred to as hierarchical imaging. This novel approach allows nondestructive 3D visualization and quantification of large microvascular networks, while retaining a precise anatomical context for ROIs scanned at very high resolution. Scans of entire mouse brain VCCs were performed at 16-μm resolution with a desktop μCT system. Custom-made navigation software with a ROI selection tool enabled the identification of anatomical brain structures and precise placement of multiple ROIs. These were then scanned at 1.4-μm voxel size using SRμCT and a local tomography setup. A framework was developed for fast sample positioning, precise selection of ROIs, and sequential high-throughput scanning of a large numbers of brain VCCs. Despite the use of local tomography, exceptional image quality was achieved with SRμCT. This method enables qualitative and quantitative assessment of vasculature at unprecedented resolution and volume with relatively high throughput, opening new possibilities to study vessel architecture and vascular alterations in models of disease.

Keywords: Hierarchical imaging; Mouse brain; Microvasculature; Synchrotron radiation; Micro-CT

Introduction

Over the last decade, the accelerated development and advances in μ-computed tomography (μCT) enabled the replication of large volumes of microvasculature ex vivo, allowing for quantitative assessment of vessel architecture in three dimensions (3D) (Bentley et al., 2002; Jorgensen et al., 1998; Plouraboue et al., 2004). Besides the descriptive and functional studies of vasculature in healthy organs and tissue, vascular alterations associated with pathology has gained increased attention, additionally fueled by the availability of genetically manipulated animals as disease models (Beckmann et al., 2003). Recently, neurodegenerative diseases, other than vascular dementia or stroke, have been associated with vascular alterations. Anatomical abnormality of the hippocampus has been suggested as a preclinical predictor for dementia onset in the elderly (Redwine et al., 2003; Vanhoesen and Hyman, 1990). In Alzheimer's disease, ischemic lesions and alterations in the microvascular network seem to play a major role in the progression of the pathology (de la Torre, 2002). It has been stated that vascular imaging systems could have a high potential to significantly accelerate the process of drug discovery and development (Beckmann et al., 2004; McDonald and Choyke, 2003).

Because pathological angiogenesis is a disease hallmark (Carmeliet and Jain, 2000), resolving microvasculature is of particular interest. However, capillaries, the smallest vascular structures in a mouse, have an inner diameter of 5–6 μm only and therefore require advanced high-resolution imaging modalities for proper visualization. Magnetic resonance angiography (MRA) and volumetric computed tomography (VCT) have been applied to demonstrate the diffuse organization of tumor vessel architecture in vivo (Kiessling et al., 2004). Despite injection of iodine or barium sulfate contrast agents, small vessels with diameters less than 20 μm were not visualized with either modality. Although in vivo experiments are the ultimate goal for clinical applications, ex vivo studies based on animal models offer some significant advantages, in particular when going to

* Corresponding author. Fax: +41 44 632 1214.
E-mail address: ralph.mueller@ethz.ch (R. Müller).
URL: http://www.bioelectronics.ethz.ch (R. Müller).
Available online on ScienceDirect (www.sciencedirect.com).

1053-8119/$ - see front matter © 2006 Elsevier Inc. All rights reserved.
doi:10.1016/j.neuroimage.2006.03.043

high-resolution imaging. Jorgensen et al. (1998) used a nearly monochromatic desktop X-ray source and optical magnification to visualize vasculature and soft tissue in isolated, fixed and stained rodent organs at a voxel size of 5 μm. They demonstrated the feasibility of local tomographic measurements with both global and local data reconstruction, however pointing out that the flux reachable with bench top X-ray sources, i.e., the number of photons produced per unit-area per second, is a limiting factor for spatial and contrast resolution. Recent studies have therefore targeted synchrotron facilities as brilliant sources for tomographic acquisition of microvasculature ex vivo. Synchrotron light is electromagnetic radiation produced by the acceleration of electrons that move near the speed of light through magnetic fields (Patterson et al., 2005). Plouraboue and colleagues performed synchrotron radiation μCT (SRμCT) on cylinders of fixed rat brain tissue, which was perfused with a combination of contrast agent and a gelatin polymer (Plouraboue et al., 2004). They used a combination of pure absorption and edge enhancement at a voxel size of 1.4 μm to visualize several cubic millimeters of microvasculature, including capillaries. Edge enhancement results from Fresnel diffraction occurring at the edges and interfaces of a slightly defocused sample (Weitkamp et al., 2002), which can be achieved by moving the sample away from the detector. In preliminary experiments, we used intact corrosion casts of whole mouse brains, a local SRμCT setup, and edge enhancement mode for visualizing and quantifying microvasculature in selected regions of interest (ROIs) at a voxel size of 1.4 μm (Heinzer et al., 2004). Vascular corrosion casts (VCCs) are a replication of the vessel lumen by filling the vasculature with a casting polymer.

Because of the limited detector size and the cubically increasing amount of image data produced as going to smaller voxel sizes, there is a trade-off between resolution and volume that can be acquired in a single scan. A desktop μCT system operated at 16-μm voxel size, for example, captures an entire mouse brain with a volume of $10 \times 16 \times 8$ mm^3, producing a 3D image of about 350 MB. A SRμCT system operated at 1.4-μm voxel size that scans a cylinder of 1.4-mm diameter and 1.4-mm height, on the other hand, produces already an image of 2 GB. Since biological studies typically target specific anatomical regions contained in a larger body of vasculature, precise ROI selection plays a pivotal role. This issue however remains problematic for several reasons, particularly for deeper brain structures. Apart from partly destroying the sample, dissecting ROIs from surrounding tissue is disadvantageous because their localization is difficult, and deformation artifacts are introduced at the cutting boundaries. If the sample is kept intact, many imaging modalities encounter difficulties because they are limited in the depth of tissue they can penetrate. Furthermore, deep anatomical structures are hidden and cannot easily be identified.

In this paper, we present a new and unique approach to systematic imaging of large volumes of vasculature at any depth of the vascular network. The method is based on the technique of modified vascular corrosion casting, desktop μCT, local SRμCT, and scanning electron microscopy (SEM) imaging, following a hierarchical and strictly nondestructive approach. Hierarchical imaging is the ability to resolve anatomical features at a variety of resolution and size scales using several complementary imaging modalities and ideally covering a few orders of magnitude in resolution (Müller and van Lenthe, 2004). Precise ROI positioning was realized through a common sample interface, a landmarking mechanism, and dedicated ROI selection software. The resulting imaging framework was optimized for high-throughput measurements and was successfully applied to scan a total of 120 regions in 30 mouse brains, resolving vascular networks ranging from cerebral and pial over intracerebral vessels down to arterioles, venules, and capillaries. Our results, which outline basic visual and quantitative evaluations on the hierarchical image data, demonstrate that the method is a powerful tool for assessing vascular architecture in animal disease models, also referred to as structural phenomics.

Materials and methods

Sample preparation and landmarking

Standard methods were used for vascular corrosion casting (Beckmann et al., 2003). APP23 transgenic mice (SturchlerPierrat et al., 1997) were deeply anesthetized and perfused by intracardial injection with a polymer resin (PU4ii, vasQtec, Zürich, Switzerland) (Krucker et al., 2006). After curing, soft tissue was macerated, followed by decalcification of surrounding bone. The cerebral vasculature, including cerebellum and olfactory bulb, was dissected from the remaining vasculature, resulting in full brain casts with a size of about $16 \times 10 \times 8$ mm. Casts exhibit even finest details like imprints of endothelial cells (Krucker et al., 2004, 2006; Reina-De La Torre et al., 1998). In order to reach better absorptions in the X-ray scans, corrosion casts were stained using osmium tetroxide (Riew and Smith, 1971).

In order to realign a sample in different imaging systems and map resulting images to a common coordinate system, a custom-made sample holder was developed. For each sample, a round table of 13-mm diameter and 3-mm height was cut from Plexiglas. Two stainless steel pins were placed in vertical orientation to the center of the table, having a length of 1.0 mm (“pin 1”) and 0.9 mm (“pin 2”), respectively, and being placed at a distance of 0.5 mm from each other (Fig. 1a). Each cast was then attached to its sample holder using instant glue (Cyanolit, 3M (Schweiz) AG, Rüschlikon, Switzerland), resulting in a sample interface for fast and reproducible sample positioning.

Desktop μCT data acquisition

A desktop μCT system (μCT 40, Scanco Medical AG, Bassersdorf, Switzerland) was used for the acquisition of whole brain samples with a nominal isotropic voxel size of 16 μm, referred to as intermediate resolution. The X-ray tube was operated at 50 kVp and 160 mA with a focal spot size of 5 μm. Per scan, 1000 projection images were acquired with an integration time of 200 ms and additional three times frame averaging for improved signal-to-noise ratio (SNR). Detailed information on the experimental setup is available elsewhere (Heinzer et al., 2004; Rüegsegger et al., 1996). Tomographic images were reconstructed on a VMS cluster (HP Alpha, HP, Palo Alto, USA) in 1024×1024 pixel matrices using a conebeam backprojection procedure. Because of the frame averaging, noise filtration could be omitted, and data were segmented directly under application of a global threshold. A bounding box was applied in order to reduce the empty space surrounding the effective brain vasculature, resulting in images of approximately $600 \times 900 \times 300$ voxels.

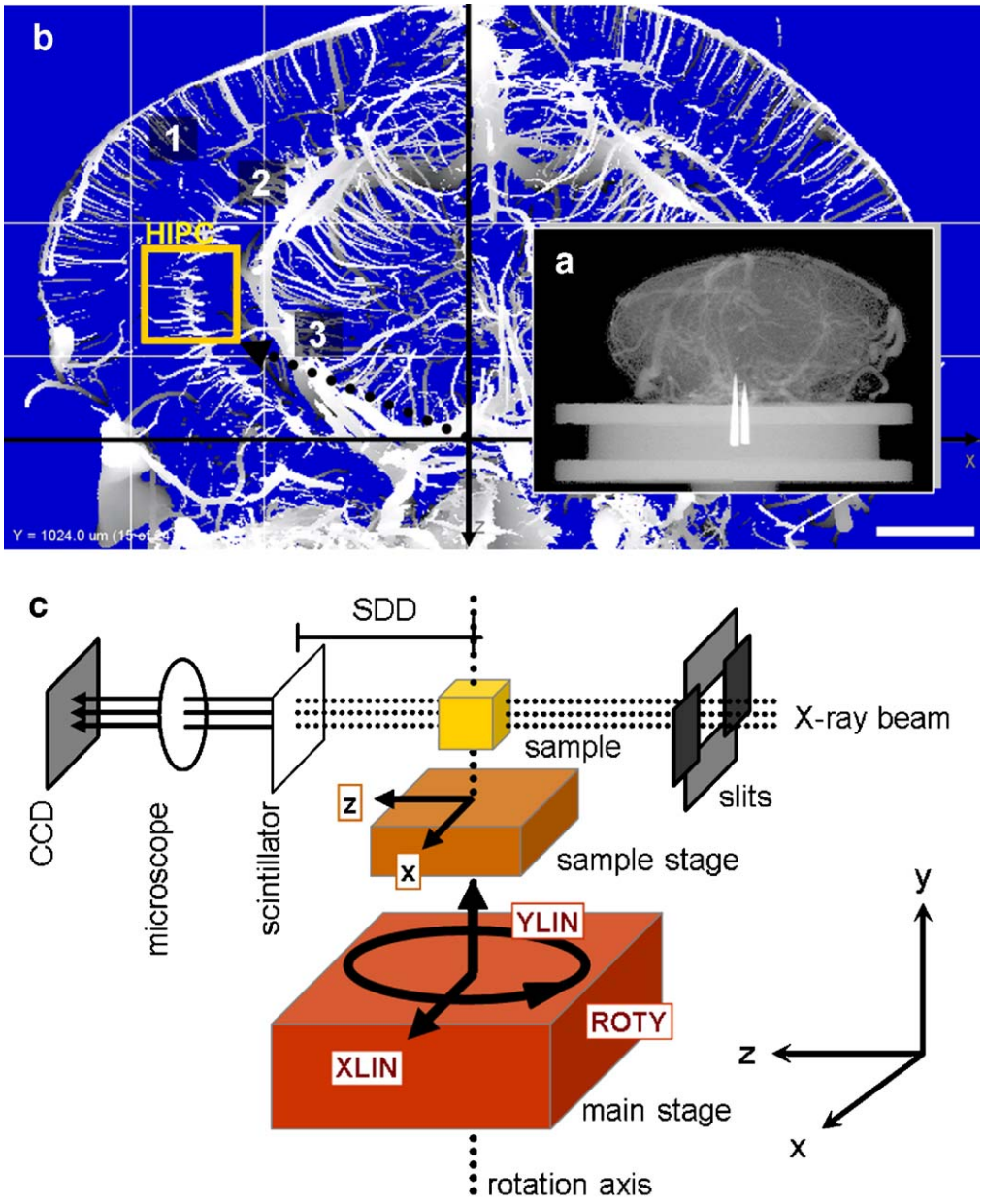

Fig. 1. Key elements for local high-resolution data acquisition. (a) Radiograph of a VCC glued on a Plexiglas stage, equipped with landmark pins. (b) Scrollable stacks of Z-buffer slices reveal anatomical brain regions like cortex (1) and hippocampus (2). ROI positions are recorded relative to landmark pins (3). (c) XTM setup for local tomography. An additional motorized sample stage (motors x, z) adds two degrees of freedom for shifting ROIs into the rotational axis, which is aligned to the center of the CCD detector via motor XLIN. Slits protect sample parts outside the field of view (FOV) from incident X-rays. The sample detector distance (SDD) determines the degree of edge enhancement.

ROI selection

Medium resolution image data were imported to custom-made ROI picking software that allows for quick browsing of the 3D data by means of scrollable stacks of overlapping Z-buffer images in dorsal, sagittal, and coronal view (Fig. 1b). Z-buffer images were produced by coloring object voxels according to the depth of their image plane, going linearly from white in the foreground to black in the background, resulting in a 3D effect (Fig. 1b). Large vessels visible in these images allowed for identification of anatomical regions, thus providing a frame of reference to the whole brain vasculature. Relative positions of ROIs (typically 3–4 per sample) with respect to the two pins in the sample holder were recorded and stored for subsequent measurement at the synchrotron beamline.

Local SRμCT data acquisition

Local tomography investigations of predefined ROIs of 1 mm^3 were performed at the X-ray Tomographic Microscopy Station of the Materials Science beamline at the Swiss Light Source (SLS) (Stampanoni et al., 2002). Exact sample positioning and sample navigation was achieved using a motorized XZ-sample translation stage mounted on top of the basic high-precision sample manipulator (Wyss et al., 2005) (Fig. 1c). This allowed keeping

the rotational axis fixed to the center of the charge-coupled device (CCD) detector, while ROIs could be shifted in the FOV of the system for local projection acquisition. Custom-made measurement software transformed ROI coordinates to match the sample alignment at the synchrotron using the landmark pin positions (Fig. 2) and allowed for unsupervised acquisition of an arbitrary number of ROIs within the sample. The monochromatic X-ray beam ($\Delta E/E = 0.014\%$) was tailored by a slits system to a profile of 1.4 mm^2 in order to confine irradiation to the scanned ROI and therefore to prevent potential deformation caused by radiation-induced heating of the cast material (Fig. 1c). Beam energy was set to 17.5 keV in order to maximize absorption contrast and to provide sufficient photon flux to penetrate the large sample. The sample detector distance (SDD) was set to 30 mm, resulting in distinct edge enhancement allowing visualization of even the smallest vascular structures (Cloetens et al., 1999; Plouraboue et al., 2004; Weitkamp et al., 2002).

After penetration of the sample, X-rays were converted into visible light by a thin Ce-doped YAG scintillator screen (Crismatec Saint-Gobain, Nemours, France). Projection images were further magnified by diffraction limited microscope optics and finally digitized by a high-resolution CCD camera (Photonic Science Ltd., East Sussex, UK) (Stampanoni et al., 2002). The optical magnification was set to 20×, and 2× on-chip binning was selected to improve the SNR, resulting in isotropic voxels of 1.4 μm for the reconstructed images. For each measurement, 1001 projections were acquired along with dark and periodic flat field images at an integration time of 2 s each. Scanning time for one volume of interest summed up to about 88 min and resulted in 2 GB of raw projection data. Data were post-processed and rearranged into flat field corrected sinograms on-line. Reconstruction of the volume of interest was performed on a 16-node Linux PC farm (Pentium 4, 2.8 GHz, 512 MB RAM) using highly optimized filtered back-projection routines and taking less than 20 min for a full dataset. Binary 3D vasculature data were extracted from 716 × 716 × 856 voxel subvolumes by Gaussian filtration and subsequent segmentation. We used a multiscale global thresholding approach, segmenting fine vessels on full scale and large vessels on downsampled image data. Downsampling smeared out small structures and thus filled holes in large vessels encountered with a single resolution threshold. The procedure was completed by application of component labeling (i.e., find the connected components of the image and retain only the largest ones) to remove remaining noise. For visualization, the data were triangulated with an extended marching cubes algorithm and surface rendered with in house software (Müller et al., 1994). In addition, Z-buffer stacks with a depth of 120 slices were produced at every 30th slices for later side-by-side comparison to μCT data in the ROI picking software.

2D verification measurements using SEM

For verification purposes, selected 2D images providing high-resolution surface data were scanned with a Baby-SEM (JEOL JSM-6360LV, JEOL, Tokyo, Japan) using tungsten filaments and a backscatter electron detector. The device was operated at low vacuum (100 Pa) with a voltage of 25 kV. This setup did not require further coating of the sample surface with a heavy metal. Gold-coated samples, as used in earlier studies, yield slightly better images but are not suitable for μCT and SRμCT measurements because of the resulting reconstruction artifacts.

Minimal and maximal vessel diameters were assessed in the SEM photomicrograph shown in Fig. 3a using the imaging software Image-Pro Plus (Media Cybernetics, Inc. Silver Spring, MD, USA). Vessel segment boundaries, defined as the section of a vessel between two consecutive ramifications, were marked manually. Only segments lying in the x/y-plane and close to the cast surface were considered, resulting in a total of 45 evaluated segments.

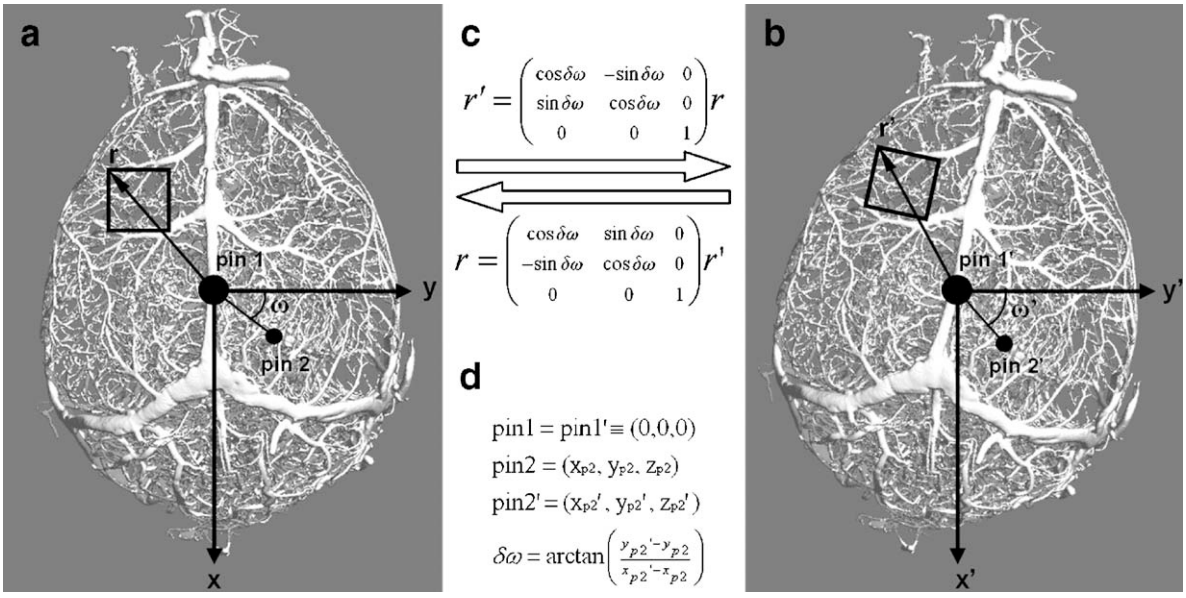

Fig. 2. Mapping of a ROI at position r between two alignments of a sample, e.g., alignment in the desktop μCT scanner (a) and at the synchrotron facility (b). In both alignments, pin 1 defines the origin of the coordinate system. The mapping of the ROI in either direction is accomplished by application of a simple rotation matrix (c). The rotation angle δω can be calculated from the coordinates of pin 2 in either alignment (d).

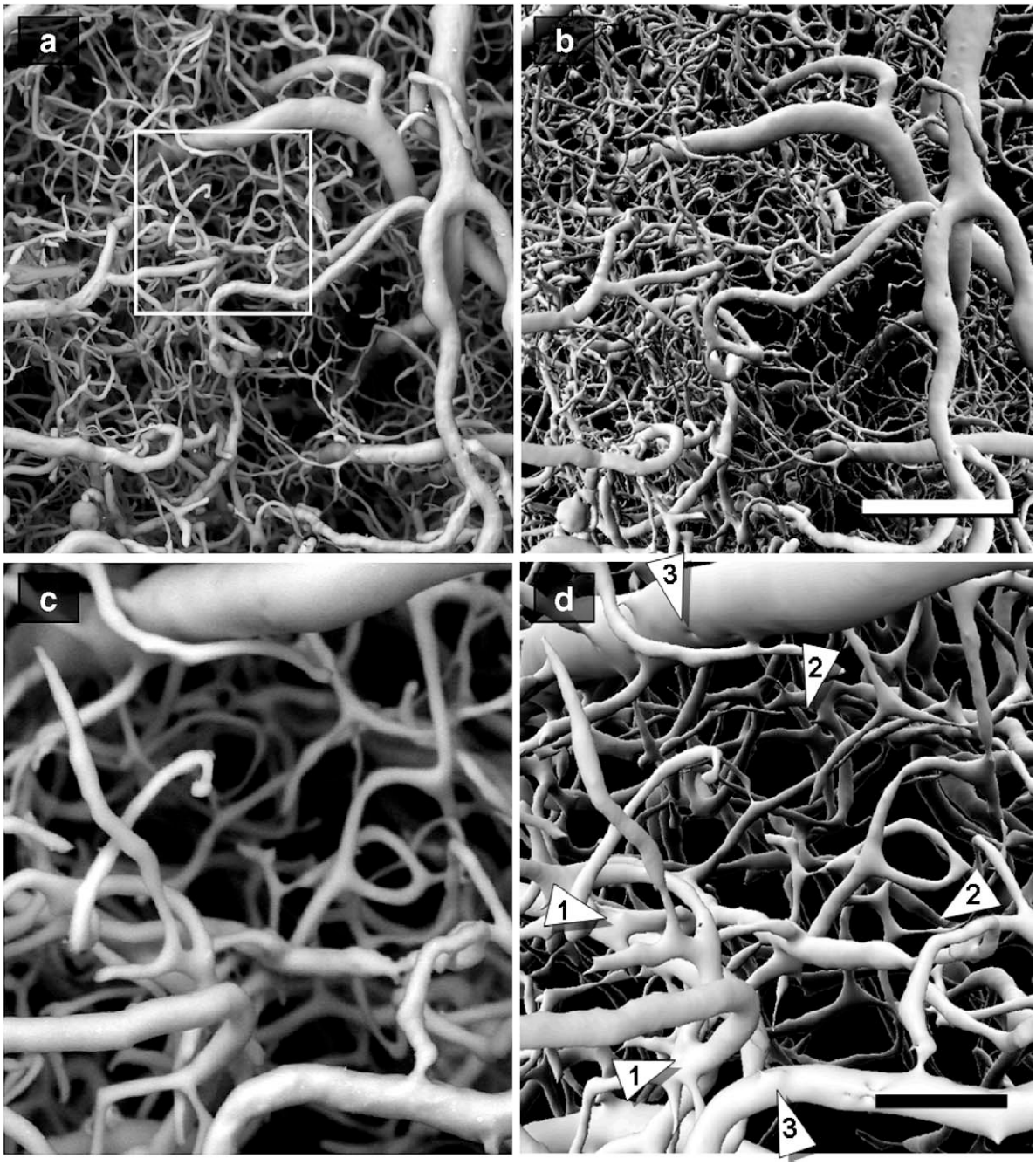

Fig. 3. Validation of SRμCT data by comparison to SEM images. (a) SEM image of vasculature at the cortical surface. (b) Surface rendered SRμCT data of the same region looking identical to the SEM data. Scale bar: 200 μm. (c) SEM detail view of the subregion outlined in panel a. (d) Surface rendered SRμCT data of the same subregion. Only at this close-up view, minor imaging artifacts become visible. The arrows indicate the three types of artifacts observed: Vessels in close proximity fuse (1), some capillaries are too thin or even disappear (2), walls of bigger vessels exhibit indents or contusions (3). Note that due to omitted sputtering and low-power SEM the vasculature appears fuzzy in panels a and c. Scale bar: 50 μm.

3D vessel morphometry

In order to demonstrate quantitative three-dimensional structure analysis, the two samples displayed in Fig. 7 were automatically evaluated using the software package IPL (Image Processing Language, Version 4.29, Scanco Medical, Bassersdorf, Switzerland) (Table 1). Parameters were adapted in analogy to terminology introduced and standardized for quantitative bone morphometry. In IPL, vessel surface area (VS) is calculated using the Marching Cubes method (Lorensen and Cline, 1987) to triangulate the surface of the binarized vessel data. Vessel volume (VV) is calculated using tetrahedrons corresponding to the enclosed volume of the triangulated surface (Guilak, 1994). Total volume (TV) is the volume of the whole examined sample. To be able to compare samples with different sizes, the normalized indices VV/TV and VS/TV are used. The specific vessel surface is then given by VS/VV. Vessel thickness (V.Th) is determined by filling maximal spheres into the vessel structure using distance transfor-

Table 1
Quantification of microvasculature shown in Fig. 7 using morphometry software

Parameter	Unit	wt animal	tg animal	Δ[%]
TV	[mm^3]	0.341	0.341	0
VV	[mm^3]	0.012	0.014	16
VS	[mm^2]	5.314	8.312	56
VV/TV	[%]	3.638	4.231	16
VS/TV	[1/mm]	15.6	24.4	56
VS/VV	[1/mm]	428.5	576.3	34
Tb.Th	[μm]	23.4	8.9	−62
Tb.Sp	[μm]	65.5	43.4	−34
Tb.N	[1/mm]	15.1	22.2	48
Conn.D	[1/mm^3]	3612	6558	82

mation (Hildebrand and Rüegsegger, 1997). Then the average thickness of all vessel voxels is calculated. Vessel spacing (V.Sp) is calculated with the same procedure as V.Th, but this time, the voxels representing nonvessel parts (background) are filled with maximal spheres. V.Sp is thus the average thickness of the intervessel cavities. Vessel number (V.N) is taken as the inverse of the mean distance between the mid-axes of the observed structure. The mid-axes of the structure are assessed from the binary 3D image using the 3D distance transformation and extracting the center points of nonredundant spheres which fill the structure completely. Then the mean distance between the mid-axes is determined in analogy to the V.Sp calculation, i.e., the separation between the mid-axes is assessed. Connectivity density (Conn.D) expresses the number of connections per cubic millimeter and is derived from the Euler number (Odgaard and Gundersen, 1993) as follows: Conn.D = (1 − Euler number)/VV. The Euler number itself is defined as the maximum number of connections that must be broken to split the structure into two parts. To compare SEM and SRμCT thickness measurements on a vessel by vessel basis, the SRμCT data were rendered by coding each thickness value with a distinct color, allowing to read out the values directly from the image. A linear regression over all data points was calculated and plotted using MATLAB (The MathWorks Inc., Natick, MA, USA) (Fig. 4).

Results

Local synchrotron tomography visualizes the capillary network nondestructively

Local tomography is a method to acquire a subregion of a sample larger than the field of view of the CCD detector (Jorgensen et al., 1998). In our approach to hierarchical assessment of intact mouse brain casts, this concept plays a fundamental role because it allows for nondestructive imaging of microvasculature at any depth of the brain. We therefore implemented local tomography at the X-ray tomographic microscopy (XTM) station (Stampanoni et al., 2002) at the Materials Science (MS) beamline of the Swiss Light Source (SLS). The standard setup was extended by two additional motors which permitted to move the sample relative to the rotation axis, while the axis itself was aligned to the center of the CCD detector, thus permitting to image any ROI within the sample (Fig. 1). Magnification, sample detector distance (SDD) and beam energy were optimized to provide sufficient contrast for the visualization of even smallest vessels like capillaries with an inner diameter of 5–6 μm only. With the current setup, each scan visualized vasculature with a cylindrical volume of 1.4-mm diameter and 1.2-mm height. To examine the quality of local SRμCT scans, surface rendered synchrotron data of the cortex surface were compared to SEM images of the same area (Fig. 3). Images from the two modalities looked almost identical, demonstrating the capabilities of the local approach. Position, thickness, connectivity, and surface topology were for the vast majority of vessels faithfully visualized (Figs. 3a, b). A linear regression on minimum and maximum vessel thickness measured in both SEM and SRμCT data yielded an R^2 value of 0.98 (Fig. 4) with a slope of 1.067 and a non significant offset of 0.002 μm. Thus, the SRμCT evaluation overestimates the SEM measurements by 6.7% but yields consistent values. Minor imaging artifacts only became visible when zooming in further on the images. Vessels in close proximity tended to fuse, some capillary segments became very thin or disappeared, and the surface of larger vessels exhibited local malformations (Figs. 3c, d).

Multimodal imaging using a single sample interface

In order to provide maximum flexibility regarding reuse of valuable cast material and repeated measurements in different imaging modalities, we sought for a sample treatment that conforms to μCT, SRμCT, and SEM imaging. We chose the newly developed PU4ii (Krucker et al., 2006) as a casting resin because it produces high-quality corrosion casts and eliminates some of the casting artifacts previously encountered with other commercially available casting materials (Lametschwandtner et al., 1990). Staining with osmium tetroxide provided good absorption contrast using μCT and SRμCT. Regarding SEM, earlier experiments required gold sputtering of the cast surface (Krucker et al., 2004). The heavy metal coating however led to artifacts in tomographic scans and disqualified the sample from further μCT and SRμCT experiments. As an interesting result, experiments with low vacuum SEM could now visualize the cast surface without further treatment (Figs. 3a, c). This makes osmium tetroxide stained

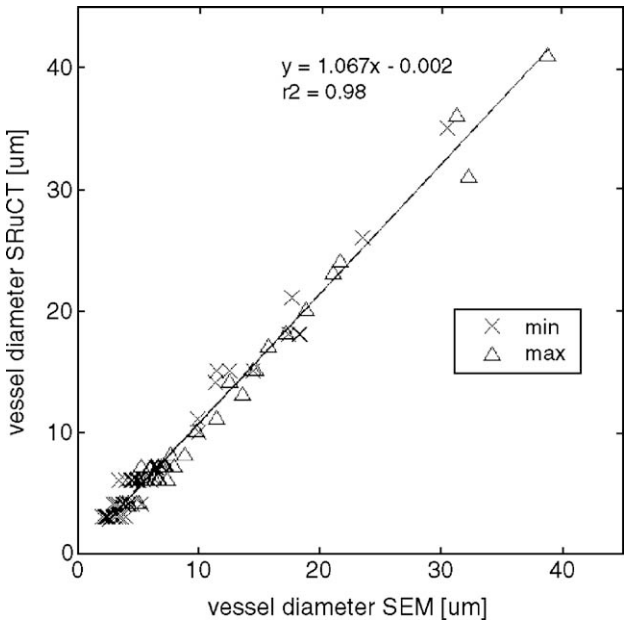

Fig. 4. Vessel by vessel comparison of thickness evaluation between SEM and SRμCT images.

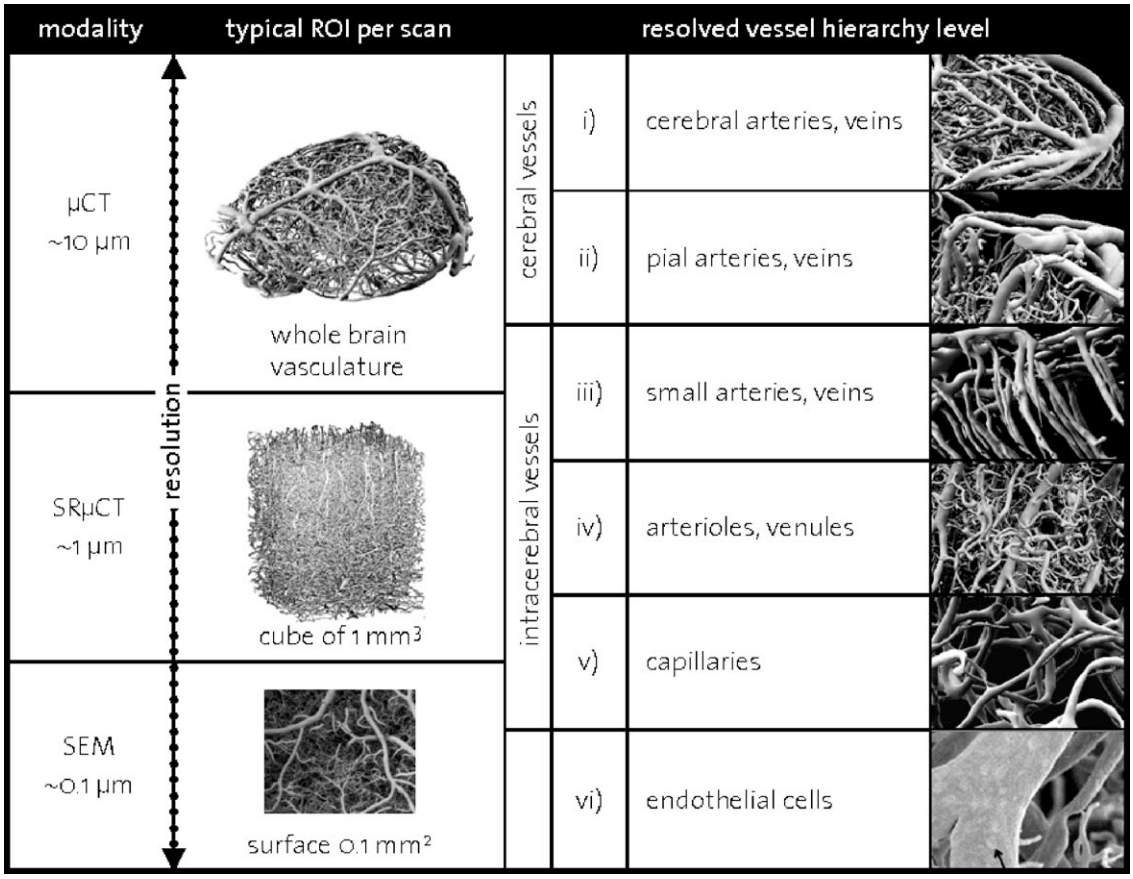

Fig. 5. Levels of hierarchy associated to image modalities used. Each order of magnitude in resolution reveals a new functional level (structure, tissue, and cell). However, the volume per scan decreases rapidly.

vascular corrosion casts a suitable medium for multimodal hierarchical imaging with μCT and SEM technology. Using this material, structures from all levels of the vessel hierarchy were visualized in detail (Figs. 1 and 5).

The problem of repositioning a sample when measuring it with different imaging modalities was solved by means of a custom-made sample holder. Once mounted, a sample was never removed from its sample holder, thus providing a firm interface for repeated, multimodal imaging. In addition, we prepared sample holders with two stainless steel pins that served as landmarks for repositioning the sample at the synchrotron facility (see Materials and methods). In order to verify that samples were correctly positioned, checks were performed routinely before each measurement, but also after data had been acquired. Z-buffer views in dorsal, sagittal, and coronal direction were used to compare the correspondence of large vessels captured by both μCT and SRμCT. The dorsal view allowed assessing rotational errors, whereas translational errors were checked in coronal and sagittal views. We found that with our landmark guided measurement protocol, targeted ROIs and measured regions matched with a precision of about 20–50 μm.

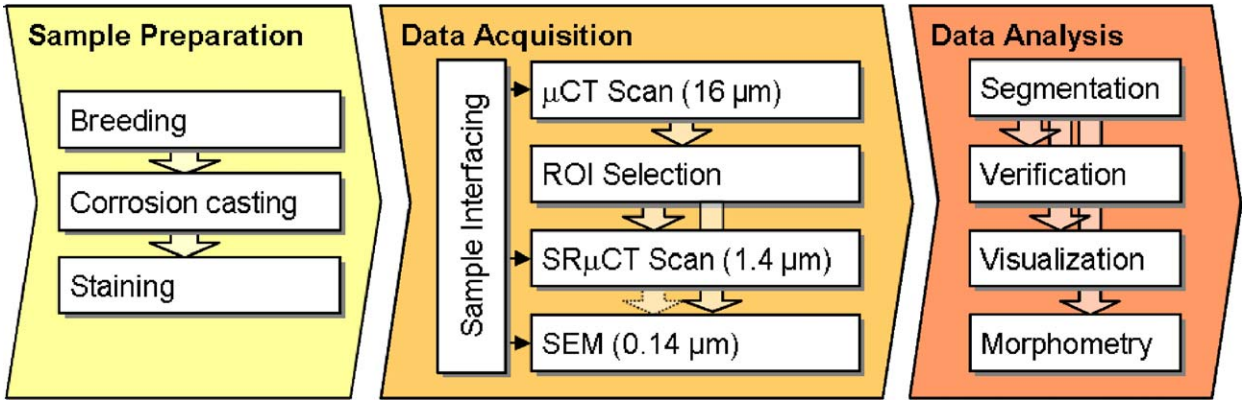

Fig. 6. Illustration of the developed hierarchical imaging framework. The straight forward approach lays the basis for high-throughput analysis. Sample interfacing plays a central role, since it provides a coordinate system for all subsequent processing steps.

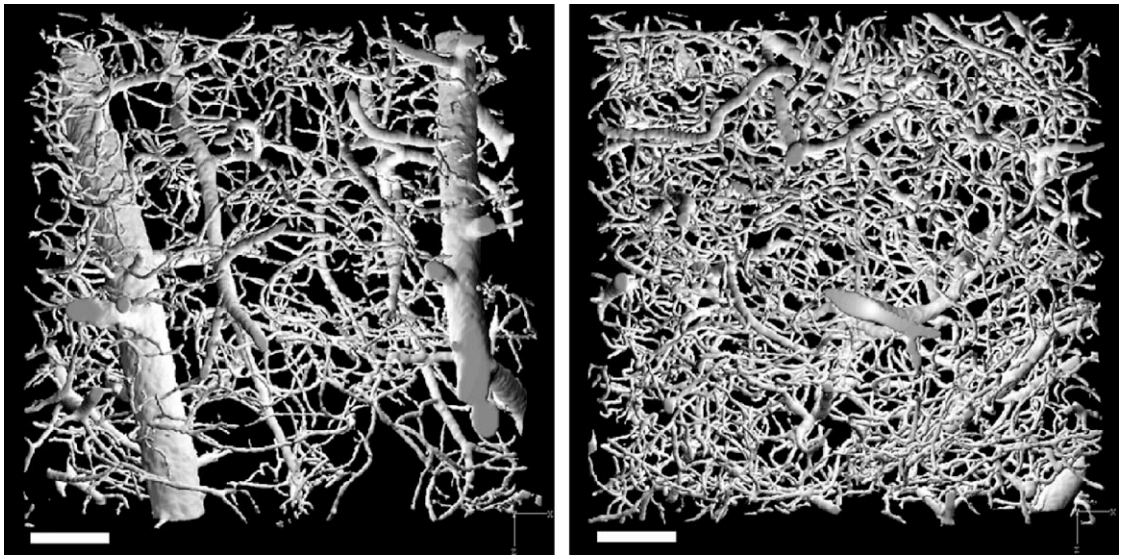

Fig. 7. Visualization of structural differences in the cortical microvasculature of a control (left) and an APP23 transgenic mouse (right). The transgenic animal exhibits decreased spacing of microvessels, which could hint an angiogenic response due to APP overexpression. Scale bars: 100 μm.

We believe that this error is small enough for an image registration algorithm to map the datasets on a micrometer scale if needed.

Framework for high-throughput measurements

Studies that use SRμCT to visualize microvasculature typically are limited to assess a small number of samples. Reasons for this are the limited availability of beamtime at the only few synchrotron facilities worldwide and the relatively complex setup involved in such experiments. Furthermore, high-resolution imaging produces very large 3D image files, typically ranging from 300 MB to 16 GB. Only rigorous automation and streamlining of the imaging process can lead to the throughput, i.e., the number of scans, needed for biological studies. One key element was to keep samples on individual sample holders (see above), allowing for quick sample positioning in all imaging systems involved. Each sample was then scanned in a "one-click" desktop μCT system (μCT 40, Scanco Medical, Switzerland), automatically reconstructed and preprocessed on a VMS cluster for ROI selection in custom-made ROI picking software. Using scrollable stacks of Z-buffer images, this software allowed for quick browsing of anatomical brain regions and precise selection of ROIs for high-resolution measurements. The software was extended to produce measurement scripts for automated SRμCT scans of an arbitrary number of ROIs within one sample, including automated tomographic reconstruction on a Linux PC farm. This setup would permit to assemble any volume of brain vasculature by subsequent scanning of adjacent regions. With our measurement protocol, sample positioning for synchrotron measurements could be reduced to less than 20 min, making it an ideal basis for upcoming fast tomography. Data segmentation and analysis were again performed on the inhouse VMS cluster in highly automated fashion. A schematic overview of the framework is given in Fig. 6.

Hierarchical imaging as a tool for structural phenomics

The proposed hierarchical imaging method was successfully used to visualize large full brain vasculature in more than 30 mice, complemented by 120 microvascular high-resolution measurements of selected ROIs. Visual analysis of high-resolution images allowed for assessment of morphological characteristics of microvasculature that did not become evident from medium resolution data. In an example of age-matched APP23 transgenic and wild-type animals, we visually observed architectural differences such as vessel spacing of the capillary bed (Fig. 7). Using quantitative morphometry, also quantitative indices were retrieved indicating, for example, a 34% decrease in vessel spacing in the transgenic animal (Table 1). Vascular features, e.g., spherical regions containing no microvasculature, could not only be identified and visualized in great detail, but also precisely localized within the context of the intact vascular entity (Fig. 8). This example illustrates how vasculature in the same sample can be assessed in top–down manner, starting at large cerebral arteries, following the transition from pial to intracerebral arteries, finally revealing the dense network of arterioles, venules, and the capillary network. The wealth of information provided in the digitized vessel data was further exploited by coloring vessels according to their thickness (Fig. 9). In good agreement with literature (Reina-De La Torre et al., 1998; Zlokovic, 2005), microvasculature observed in the left frontal cortex was organized in vertically penetrating intracerebral arteries and horizontally layer-wise branching arterioles and capillaries.

Discussion

Hierarchical imaging is an effective tool to assess large vascular networks

The results presented in this paper show the new possibilities that arise from assessing vascular corrosion casts with hierarchical imaging. We presented its application to the mouse brain, which is probably the most challenging organ due to its complex organization. The technique, however, can equally be applied to other structures such as tumors or the cardiovascular system. The proposed multimodal framework enables top–down imaging and analysis of vasculature in a single sample, visualizing all levels of

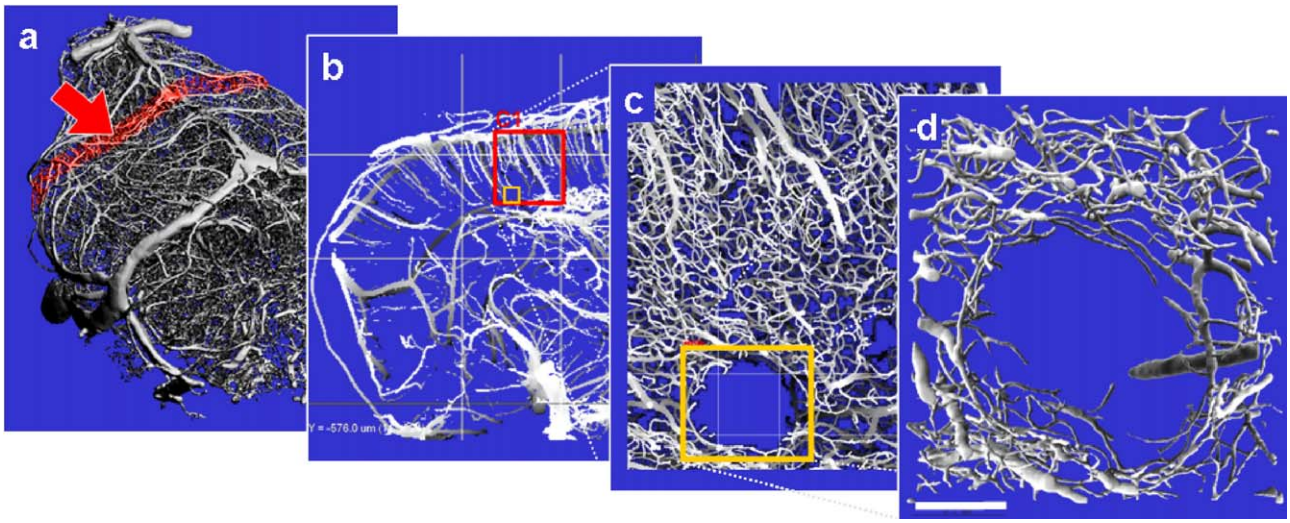

Fig. 8. Hierarchical investigation of vascular architecture. (a) Intact mouse brain vasculature scanned at medium resolution (16-μm voxel size) using a desktop μCT system. (b) Z-buffer slice of the section marked red in panel (a), revealing the frontal cortex. The red square labeled "C1" denotes a region of interest (ROI) which was measured using SRμCT. (c) Z-buffer slice of SRμCT high-resolution data visualizing intracerebral arteries and the capillary network. The latter is not visualized in the medium resolution data (b) but provides essential structural characteristics of the vasculature, as for example the microinfarct marked by the red rectangle. (d) Surface rendering of the infarct region marked in panel (c) suitable for detailed and high-quality 3D analysis. Scale bar: 100 μm.

the vessel hierarchy at unprecedented resolution and size, including the capillary bed (Fig. 5). Desktop μCT captures all large cerebral arteries, pial arteries and large intracerebral arteries, but cannot resolve smaller vessels such as capillaries. Local SRμCT is able to close this gap at the intracerebral level and gives detailed insight to the organization of the microvascular network in selected ROIs (Figs. 5 and 8). The advantages that arise from possessing a map of the overall structure of the vasculature under investigation are manifold. Desktop μCT scans that revealed the entire network of large vessels were not only crucial for ROI selection (Fig. 1b) but also provided the means to verify the exact location of high-resolution data. Furthermore, this medium resolution data unraveled the context of localized features when studying microvascular architecture (Fig. 8). Selected cubes of microvasculature from within anatomical regions such as hippocampus and cortex were acquired at the synchrotron facility with a local tomographic approach, which was optimized for fast sample positioning and automated acquisition of multiple ROIs. Interestingly, this setup allows for automated acquisition of adjacent regions, which could be assembled to a larger volume by means of image registration software. At a voxel size of 1.4 μm, even smallest vessels of only a few microns in diameter were visualized. The high fidelity of these images was demonstrated and verified by direct comparison to SEM images. Although the current method focuses on small animal imaging ex vivo, the hierarchical approach could be extended to incorporate modalities such as micromagnetic resonance imaging (μMRI) or high-resolution CT systems for preclinical (Kiessling et al., 2004) and even clinical in vivo applications (McDonald and Choyke, 2003).

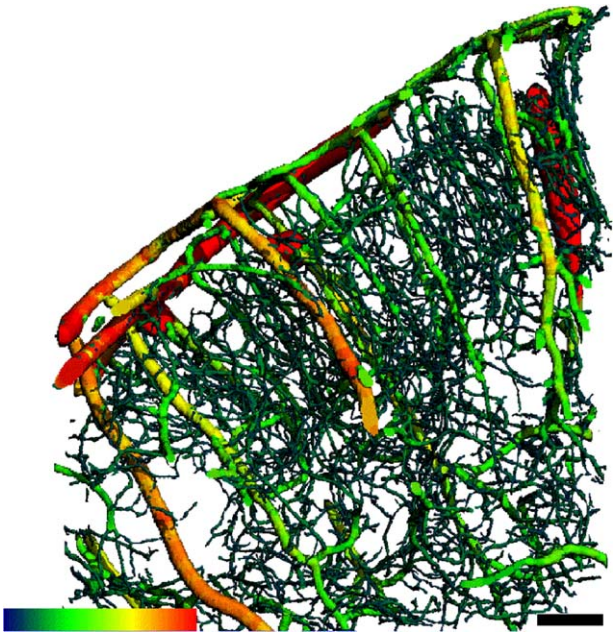

Fig. 9. Portion of microvasculature from the left frontal cortex. The color coding reflects vessel thickness, ranging in the current example from about 5 μm (dark green) to 30 μm (red). Scale bar: 100 μm.

Resolving microvasculature with local tomography

In this paper, we used local tomography as a powerful method to image arbitrary regions within corrosion casts at very high image quality. The nondestructive nature of this approach provides improved stability to the cast material in the ROI during image acquisition, thus reducing potential deformation artifacts that may be caused by radiation-induced heating of the cast material. Intact cast material can be reused for follow-up studies or verification measurements, thus minimizing the number of animals needed for a study.

In agreement with other publications (Anastasio et al., 2004; Jorgensen et al., 1998), we obtained useful data even when reconstructing our local data with a global method. The effect of concentric gradients was not as pronounced as described by Jorgensen et al. (1998), which might be due to the fact that

vasculature is a sparse structure that contributes relatively little absorption from outside the field of view. However, we encountered problems with a regular buckling pattern visible in reconstructed slice data, which after global thresholding resulted in small holes visible throughout larger vessels. This would disqualify the data from quantitative morphometrical analysis. When working with datasets in the gigabyte range, complex thresholding algorithms like curve evolution (Lorigo et al., 2001) or gradient-based approaches (Zana and Klein, 2001) are challenging because of excessive computing time and memory requirements. We addressed the problem by using a simple and efficient multiscale global threshold procedure. Minor artifacts (Fig. 3d) however remain: Gaussian filtration used in the segmentation procedure is important for noise suppression, vessel boundaries however get blurred, leading to fusion of very close vessels. Likewise, very thin vessels are slightly washed out and have a tendency to fall below the global threshold, resulting in capillary segments that turn out too thin or disappear. Nevertheless, since these artifacts were limited to a few vessels only, we conclude that local synchrotron tomography is capable of visualizing the capillary network with very high fidelity, close to that of images known from SEM.

Hierarchical imaging provides data for quantitative morphometry

Apart from the valuable information gained from visual inspection of high-quality vessel data, the power of digital 3D images lies in its potential for quantitative characterization of tissues (Bentley et al., 2002; Hildebrand et al., 1999). Such image data can be evaluated with a minimum of user interaction in a highly automated fashion (Müller and van Lenthe, 2004). The need to assess vessel morphometry has been stated for several research fields. In pharmaceutical research, better knowledge of vessel architecture and vessel alterations evoked by pathological conditions could support drug discovery and drug monitoring (Beckmann et al., 2004). Prominent pharmaceutical fields include dementia (Krucker et al., 2004) and tumor therapy (McDonald and Choyke, 2003). Regarding tissue engineering applications that deal with angiogenesis, vessel quantification is crucial to judge different treatments (Brey et al., 2002). In addition to classical quantitative morphometry, a wealth of structural parameters can be extracted from 3D vessel data through vascular tree analysis (Wan et al., 2002). Quantification at well-defined levels of the vessel hierarchy or even assessment of local properties of single capillaries could elucidate vessel function in health and disease. With the hierarchical method, a variety of samples has been collected to investigate vascular alterations in animal disease models. Extensive morphometrical analysis of this data will show the capability of the approach to assess structural changes in terms of numbers and statistics.

In conclusion, we have introduced a novel approach to systematic assessment of brain vasculature in fully nondestructive fashion. Through combination of desktop μCT, SRμCT, and SEM imaging, the method reveals vascular features at a wide range of scales with unprecedented resolution and size, thereby never losing track of the structure in its entirety. Using this approach, it would in principle be possible to successively subsample the whole brain microvasculature at 1-μm resolution. With its capability to elucidate vascular network structure at all levels from cerebral arteries down to the capillary bed, the proposed hierarchical method could open new avenues on how to asses vascular architecture in small animals, with impact on drug detection and drug monitoring.

Acknowledgments

We would like to thank Adriane Mosley and Sarah Morgan (The Scripps Research Institute, San Diego, USA) for their help breeding the animals. We also thank Urs Ziegler (Anatomisches Institut, University of Zürich, Zürich, Switzerland) for his help acquiring the SEM images. We also thank Dr. Amela Groso for her support during the experiments at the SLS. This work was supported by Novartis, PSI, and the Swiss National Science Foundation (SNF 620-58097.99).

References

Anastasio, M.A., Shi, D.X., De Carlo, F., Pan, X.C., 2004. Analytic image reconstruction in local phase-contrast tomography. Phys. Med. Biol. 49 (1), 121–144.

Beckmann, N., Schuler, A., Mueggler, T., Meyer, E.P, Wiederhold, K.H., Staufenbiel, M., Krucker, T., 2003. Age-dependent cerebrovascular abnormalities and blood flow disturbances in APP23 mice modeling Alzheimer's disease. J. Neurosci. 23 (24), 8453–8459.

Beckmann, N., Laurent, D., Tigani, B., Panizzutti, R., Rudin, M., 2004. Magnetic resonance imaging in drug discovery: lessons from disease areas. Drug Discov. Today 9 (1), 35–42.

Bentley, M.D., Ortiz, M.C., Ritman, E.L., Romero, J.C., 2002. The use of microcomputed tomography to study microvasculature in small rodents. Am. J. Physiol.: Regul., Integr. Comp. Physiol. 282 (5), R1267–R1279.

Brey, E.M., King, T.W., Johnston, C., McIntire, L.V., Reece, G.P., Patrick, C.W. Jr., 2002. A technique for quantitative three-dimensional analysis of microvascular structure. Microvasc. Res. 63 (3), 279–294.

Carmeliet, P., Jain, R.K., 2000. Angiogenesis in cancer and other diseases. Nature 407 (6801), 249–257.

Cloetens, P., Ludwig, W., Baruchel, J., Guigay, J.P., Pernot-Rejmankova, P., Salome-Pateyron, M., Schlenker, M., Buffiere, J.Y., Maire, E., Peix, G., 1999. Hard X-ray phase imaging using simple propagation of a coherent synchrotron radiation beam. J. Phys. D: Appl. Phys. 32 (10A), A145–A151.

de la Torre, J.C., 2002. Alzheimer disease as a vascular disorder—Nosological evidence. Stroke 33 (4), 1152–1162.

Guilak, F., 1994. Volume and surface area measurement of viable chondrocytes in situ using geometric modelling of serial confocal sections. J. Microsc. 173 (Pt. 3), 245–256.

Heinzer, S., Krucker, T., Stampanoni, M., Abela, R., Meyer, E.P., Schneider, P., Müller, R., 2004. Hierarchical bioimaging and quantification of vasculature in disease models using corrosion casts and microcomputed tomography. In: Bonse, U (Ed.), Proc. SPIE, vol. 5535. SPIE, Bellingham, WA, USA, pp. 65–76.

Hildebrand, T., Rüegsegger, P., 1997. A new method for the model independent assessment of thickness in three-dimensional images. J. Microsc. 185, 67–75.

Hildebrand, T., Laib, A., Muller, R., Dequeker, J., Ruegsegger, P., 1999. Direct three-dimensional morphometric analysis of human cancellous bone: microstructural data from spine, femur, iliac crest, and calcaneus. J. Bone Miner. Res. 14 (7), 1167–1174.

Jorgensen, S.M., Demirkaya, O., Ritman, E.L., 1998. Three-dimensional imaging of vasculature and parenchyma in intact rodent organs with X-ray micro-CT. Am. J. Physiol. 275 (3 Pt. 2), H1103–H1114.

Kiessling, F., Greschus, S., Lichy, M.P., Bock, M., Fink, C., Vosseler, S., Moll, J., Mueller, M.M., Fusenig, N.E., Traupe, H., et al., 2004. Volumetric computed tomography (VCT): a new technology for noninvasive, high-resolution monitoring of tumor angiogenesis. Nat. Med. 10 (10), 1133–1138.

Krucker, T., Schuler, A., Meyer, E.P., Staufenbiel, M., Beckmann, N., 2004. Magnetic resonance angiography and vascular corrosion casting as tools in biomedical research: application to transgenic mice modeling Alzheimer's disease. Neurol. Res. 26 (5), 507–516.

Krucker, T., Lang, A., Meyer, E.P., 2006. New polyurethane-based material for vascular corrosion casting with improved physical and imaging characteristics. Microsc. Res. Tech. 69, 138–147.

Lametschwandtner, A., Lametschwandtner, U., Weiger, T., 1990. Scanning electron-microscopy of vascular corrosion casts-technique and applications-updated review. Scanning Microsc. 4 (4), 889–941.

Lorensen, W.E., Cline, H.E., 1987. Marching cubes: a high resolution 3D surface construction algorithm. Comput. Graph. 21 (4), 163–169.

Lorigo, L.M., Faugeras, O.D., Grimson, W.E.L., Keriven, R., Kikinis, R., Nabavi, A., Westin, C.F., 2001. CURVES: curve evolution for vessel segmentation. Med. Image Anal. 5 (3), 195–206.

McDonald, D.M., Choyke, P.L., 2003. Imaging of angiogenesis: from microscope to clinic. Nat. Med. 9 (6), 713–725.

Müller, R., van Lenthe, G.H., 2004. 3-D microcomputed tomography: a new method to assess bone microarchitecture. Medicographia 26 (3), 285–293.

Müller, R., Hildebrand, T., Rüegsegger, P., 1994. Non-invasive bone biopsy: a new method to analyse and display the three-dimensional structure of trabecular bone. Phys. Med. Biol. 39 (1), 145–164.

Odgaard, A., Gundersen, H.J., 1993. Quantification of connectivity in cancellous bone, with special emphasis on 3-D reconstructions. Bone 14 (2), 173–182.

Patterson, B.D., Abela, R., Auderset, H., Chen, Q., Fauth, F., Gozzo, F., Ingold, G., Kuhne, H., Lange, M., Maden, D., et al., 2005. The materials science beamline at the Swiss light source: design and realization. Nucl. Instrum. Methods Phys. Res., Sect. A, Accel. Spectrom. Detect. Assoc. Equip. 540 (1), 42–67.

Plouraboue, F., Cloetens, P., Fonta, C., Steyer, A., Lauwers, F., Marc-Vergnes, J.P., 2004. X-ray high-resolution vascular network imaging. J. Microsc. 215 (Pt2), 139–148.

Redwine, J.M., Kosofsky, B., Jacobs, R.E., Games, D., Reilly, J.F., Morrison, J.H., Young, W.G., Bloom, F.E., 2003. Dentate gyrus volume is reduced before onset of plaque formation in PDAPP mice: a magnetic resonance microscopy and stereologic analysis. Proc. Natl. Acad. Sci. U. S. A. 100 (3), 1381–1386.

Reina-De La Torre, F., Rodriguez-Baeza, A., Sahuquillo-Barris, J., 1998. Morphological characteristics and distribution pattern of the arterial vessels in human cerebral cortex: a scanning electron microscope study. Anat. Rec. 251 (1), 87–96.

Riew, C.K., Smith, R.W., 1971. Modified osmium tetroxide stain for microscopy of rubber-toughened resins. J. Polym. Sci., A-1, Polym. Chem. 9 (9) ((2739-&)).

Rüegsegger, P., Koller, B., Müller, R., 1996. A microtomographic system for the nondestructive evaluation of bone architecture. Calcif. Tissue Int. 58 (1), 24–29.

Stampanoni, M., Borchert, G., Wyss, P., Abela, R., Patterson, B., Hunt, S., Vermeulen, D., Ruegsegger, P., 2002. High resolution X-ray detector for synchrotron-based microtomography. Nucl. Instrum. Methods Phys. Res., Sect. A, Accel. Spectrom. Detect. Assoc. Equip. 491 (1–2), 291–301.

SturchlerPierrat, C., Abramowski, D., Duke, M., Wiederhold, K.H., Mistl, C., Rothacher, S., Ledermann, B., Burki, K., Frey, P., Paganetti, P.A., et al., 1997. Two amyloid precursor protein transgenic mouse models with Alzheimer disease-like pathology. Proc. Natl. Acad. Sci. U. S. A. 94 (24), 13287–13292.

Vanhoesen, G.W., Hyman, B.T., 1990. Hippocampal-formation-anatomy and the patterns of pathology in Alzheimers-disease. Prog. Brain Res. 83, 445–457.

Wan, S.Y., Ritman, E.L., Higgins, W.E., 2002. Multi-generational analysis and visualization of the vascular tree in 3D micro-CT images. Comput. Biol. Med. 32 (2), 55–71.

Weitkamp, T., Rau, C., Snigirev, A.A., Benner, B., Günzler, T.F., Kuhlmann, M., Schroer, C.G., 2002. In-line phase contrast in synchrotron-radiation microradiography and tomography. In: Bonse, U (Ed.), Proceedings SPIE. San Diego, SPIE, pp. 92–102.

Wyss, P., Thurner, P., Bronnimann, R., Sennhauser, U., Stampanoni, M., Abela, R., Muller, R., 2005. Sample handler for X-ray tomographic microscopy and image-guided failure assessment. Rev. Sci. Instrum. 76 (7), 076106.1–076106.3.

Zana, F., Klein, J.C., 2001. Segmentation of vessel-like patterns using mathematical morphology and curvature evaluation. IEEE Trans. Image Process. 10 (7), 1010–1019.

Zlokovic, B.V., 2005. Neurovascular mechanisms of Alzheimer's neurodegeneration. Trends Neurosci. 28 (4), 202–208.